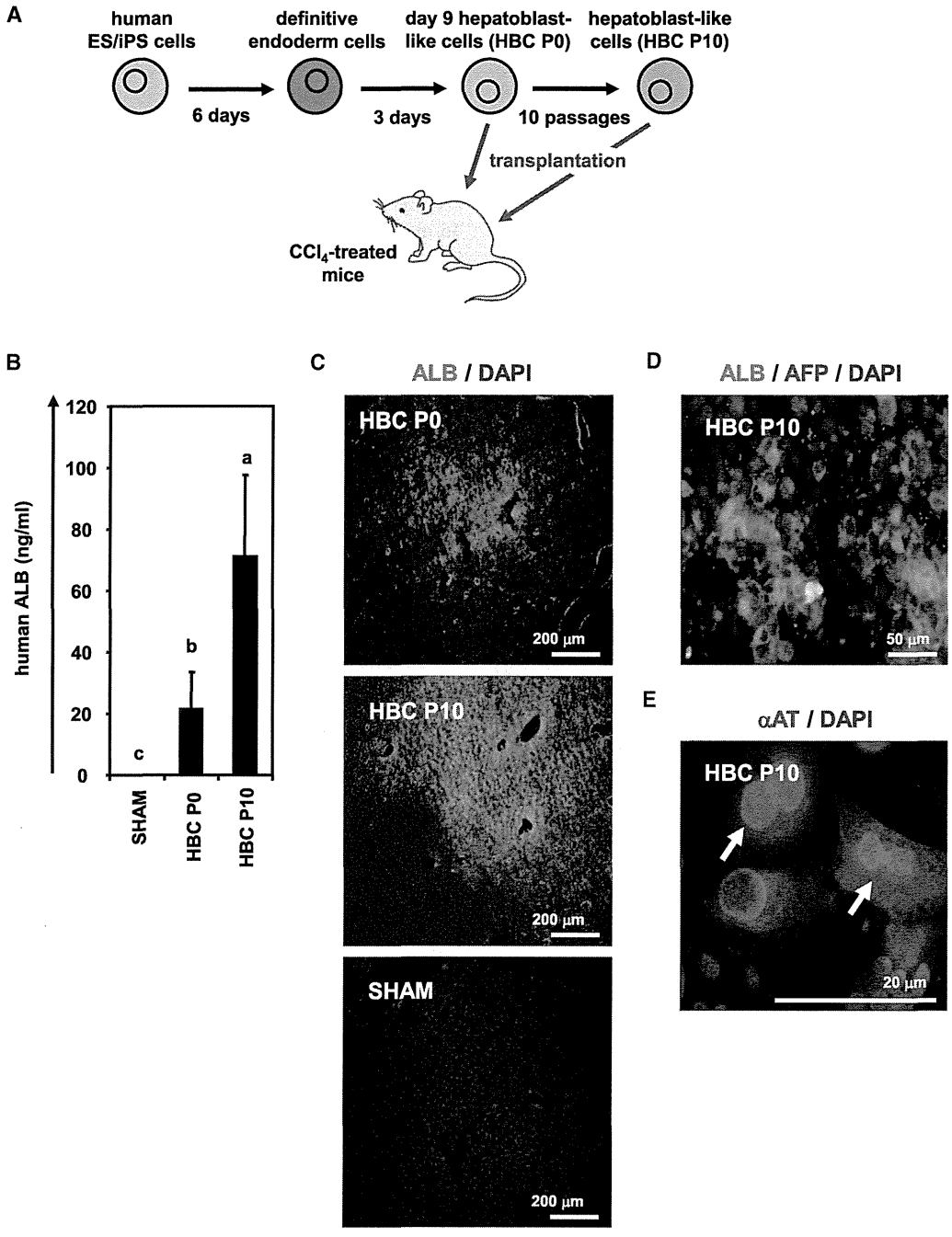

Figure 5. The hESC-Derived HBCs Were Integrated into the Mouse Liver Parenchyma

(A) The procedure for transplantation of the hESC (H9)-derived HBC P0 and HBC P10 into CCl_4 (4 ml/kg)-treated Rag2/IL2 receptor gamma double-knockout mice is presented schematically.

(B) The human ALB level in recipient mouse serum was measured at 2 weeks after transplantation. Data represent the mean ± SD from six to eight mice in each group. Statistical significance was evaluated by ANOVA followed by Bonferroni post hoc tests to compare all groups. Groups that do not share the same letter are significantly different from each other ($p < 0.05$).

(C) Expressions of the ALB (green) in the liver of transplanted mice were examined by immunohistochemistry at 2 weeks after transplantation.

(D and E) The expressions of AFP (red), ALB (green) (D), and αAT (red) (E) were examined by immunohistochemistry at 2 weeks after hESC-derived HBC P10 transplantation. White arrows show transplanted cells, which have double nuclei.

See also Tables S2 and S3.

et al., 2011; Takayama et al., 2011; Tashiro et al., 2010). The VP titer was determined by using a spectrophotometric method.

Flow Cytometry

Single-cell suspensions of the hPSC-derived cells were fixed with 4% paraformaldehyde (PFA) at 4°C for 10 min and then incubated with the primary antibody (described in Table S2), followed by the secondary antibody (described in Table S3). Control cells were incubated with anti-mouse, goat, or rabbit immunoglobulin (Ig) G antibodies (Santa Cruz Biotechnology) and then incubated with the secondary antibody. Flow cytometry analysis was performed using a fluorescence-activated cell sorting (FACS) LSR Fortessa flow cytometer (BD Biosciences). Cell sorting was performed using a FACS Aria (BD Biosciences).

RNA Isolation and RT-PCR

Total RNA was isolated from hPSCs and their derivatives using ISOGENE (Nippon Gene). cDNA was synthesized using 500 ng of total RNA with a Superscript VILO cDNA synthesis kit (Invitrogen). Real-time RT-PCR was performed with SYBR green PCR Master Mix (Applied Biosystems) using an Applied Biosystems StemOnePlus real-time PCR systems. Relative quantification was performed against a standard curve, and the values were normalized against the input determined for the housekeeping gene, glyceraldehyde 3-phosphate dehydrogenase. The primer sequences used in this study are described in Table S4. In addition, we confirmed that every beta integrin primer used in this manuscript showed a similar amplification efficacy (Table S5). The amplification efficiency was calculated from the slope of the standard curve according to the following formula: e = 10^(−1/slope)-1. Every beta integrin primer used in this manuscript showed a similar amplification efficacy.

Immunohistochemistry

The cells were fixed with 4% PFA for 15 min and then blocked with PBS containing 2% FBS, 2% bovine serum albumin (BSA), and 0.1% Triton X-100 (Wako Pure Chemicals Industries) for 1 hr. The cells were incubated with primary antibody (described in Table S2) at 4°C for overnight, followed by incubation with a secondary antibody (described in Table S3) at room temperature for 1 hr. Nuclei were counterstained with DAPI (blue).

ELISA

The hPSC-derived HBC P0, HBC P10, and HBC clone were differentiated into the hepatocyte-like cells as described in Figure 4A. The culture supernatants, which were incubated for 24 hr after fresh medium was added, were collected and analyzed for the amount of ALB secretion by ELISA. ELISA kits for ALB were purchased from Bethyl Laboratories. The amount of ALB secretion was calculated according to each standard followed by normalization to the protein content per well. The human ALB amount in mice serum was also examined by ELISA.

Transplantation of the hESC-Derived HBCs

The hESC-derived HBCs were dissociated using accutase and then suspended with maintenance DMEM/F12 medium without serum. Eight- to 10-week-old Rag2/IL2Rg double-knockout mice were prepared. The hESC-derived HBCs (1×10^6 cells) were transplanted 24 hr after administration of CCl_4 (4 ml/kg) by intrasplenical injection. Recipient mouse liver and blood were harvested at 2 weeks after transplantation. The livers were fixed with 4% PFA and processed for immunohistochemistry. Human hepatocytes producing the ALB, AFP, and αAT protein were identified in mouse liver by an antibody specifically recognizing human but not mouse albumin. In addition, serum was extracted and subjected to ELISA analysis. All animal experiments were conducted in accordance with institutional guidelines.

Urea Secretion

The hPSC-derived HBC P0, HBC P10, and HBC clone were differentiated into hepatocyte-like cells as described in Figure 4A. The culture supernatants, which were incubated for 24 hr after fresh medium was added, were collected and analyzed for the amount of urea secretion. The urea measurement kits were purchased from BioAssay Systems. The amount of urea secretion was calculated according to each standard followed by normalization to the protein content per well. In Figure S5B, both the HBC-derived hepatocyte-like cells and primary human hepatocytes (PHs) (three lots of cryopreserved human hepatocytes were used), that were cultured for 48 hr after the cells were plated (PH 48 hr), were cultured in HCM (containing glutamine) or DMEM (not containing glutamine; Wako) in the presence or absence of 1 mM ammonium chloride (NH_4Cl, Wako) for 24 hr, and then the amount of urea secretion was measured.

Primary Human Hepatocytes

Three lots of cryopreserved human hepatocytes (lot Hu8072 [CellzDirect], HC2-14, and HC10-101 [Xenotech]) were used. The vials of hepatocytes were rapidly thawed in a shaking water bath at 37°C; the contents of the vial were emptied into prewarmed Cryopreserved Hepatocyte Recovery Medium (Gibco) and the suspension was centrifuged at 100 g for 10 min at room temperature. The hepatocytes were seeded at 1.25×10^5 cells/cm^2 in HCM (Lonza) containing 10% fetal calf serum (FCS) (Gibco) onto type I collagen-coated 12-well plates. The medium was replaced with hepatocyte culture medium containing 10% FCS 6 hr after seeding. The hepatocytes, which were cultured 48 hr after plating the cells, were used in the experiments.

Adhesion-Blocking Assay Using Integrin Antibody

Twelve-well plates were coated with human recombinant LN111, 211, 411, or 511 (all from BioLamina) and blocked by 1% heat-denatured BSA containing PBS. The hESC-derived single cells were incubated with function-blocking antibodies to integrin α6 and β1 (at the concentrations as recommended by the manufacturer) for 30 min, plated on a human LN111-coated 12-well dish, and allowed to adhere for 1 hr at 37°C. After unattached cells were removed, the remaining adherent cells were fixed for 20 min with 5% glutaraldehyde. The hESC-derived cells that had adhered to the wells were stained with 200 μl of 0.3% crystal violet (Wako) solution at room temperature for 15 min. Excess crystal violet was then removed, and the wells were washed three times. Fixed crystal violet was solubilized in 200 μl of 100% ethanol at room

temperature for 15 min. Cell viability was estimated by measuring the absorbance at 595 nm of each well using a microtiter plate reader (Sunrise, Tecan).

CYP Activity

To measure the CYP1A2, 2C9, and 3A4 activity of the cells, we performed lytic assays by using P450-GloTM CYP1A2, 2C9, and 3A4 Assay Kits (Promega), respectively. We measured the fluorescence activity with a luminometer (Lumat LB 9507; Berthold) according to the manufacturer's instructions. The CYP activity was normalized with the protein content per well.

Karyotyping

This experiment was carried out at Chromosome Science Labo.

Cell Viability Tests

Cell viability was assessed by using a WST-8 assay kit (Dojindo), and the results are presented in Figure S5C. After treatment with test compounds, such as acetaminophen (Wako) and troglitazone (Wako) for 24 hr, the cell viability was measured. The control cells were incubated in the absence of test compounds and were considered to have 100% viability value. Controls were treated with DMSO (final concentration 0.1%).

SUPPLEMENTAL INFORMATION

Supplemental Information includes five figures and five tables and can be found with this article online at http://dx.doi.org/10.1016/j.stemcr.2013.08.006.

ACKNOWLEDGMENTS

We thank Yasuko Hagihara for her excellent technical support. H.M., K.K., and T.H. were supported by grants from the Ministry of Health, Labor, and Welfare of Japan. H.M. was also supported by the Project for Technological Development of the Japan Science and Technology Agency (JST) and by the Uehara Memorial Foundation. F.S. was supported by Program for Promotion of Fundamental Studies in Health Sciences of the National Institute of Biomedical Innovation. K.T. and Y.N. are Research Fellows of the Japan Society for the Promotion of Science.

Received: June 6, 2013
Revised: August 27, 2013
Accepted: August 27, 2013
Published: October 3, 2013

REFERENCES

Clément, B., Rescan, P.Y., Baffet, G., Loréal, O., Lehry, D., Campion, J.P., and Guillouzo, A. (1988). Hepatocytes may produce laminin in fibrotic liver and in primary culture. Hepatology *8*, 794–803.

Couvelard, A., Bringuier, A.F., Dauge, M.C., Nejjari, M., Darai, E., Benifla, J.L., Feldmann, G., Henin, D., and Scoazec, J.Y. (1998). Expression of integrins during liver organogenesis in humans. Hepatology *27*, 839–847.

Hay, D.C., Zhao, D., Fletcher, J., Hewitt, Z.A., McLean, D., Urruticoechea-Uriguen, A., Black, J.R., Elcombe, C., Ross, J.A., Wolf, R., and Cui, W. (2008). Efficient differentiation of hepatocytes from human embryonic stem cells exhibiting markers recapitulating liver development in vivo. Stem Cells *26*, 894–902.

Inamura, M., Kawabata, K., Takayama, K., Tashiro, K., Sakurai, F., Katayama, K., Toyoda, M., Akutsu, H., Miyagawa, Y., Okita, H., et al. (2011). Efficient generation of hepatoblasts from human ES cells and iPS cells by transient overexpression of homeobox gene HEX. Mol. Ther. *19*, 400–407.

Kamiya, A., Kakinuma, S., Yamazaki, Y., and Nakauchi, H. (2009). Enrichment and clonal culture of progenitor cells during mouse postnatal liver development in mice. Gastroenterology *137*, 1114–1126.

Liu, H., Kim, Y., Sharkis, S., Marchionni, L., and Jang, Y.Y. (2011). In vivo liver regeneration potential of human induced pluripotent stem cells from diverse origins. Sci. Transl. Med. *3*, 82ra39.

Makino, H., Toyoda, M., Matsumoto, K., Saito, H., Nishino, K., Fukawatase, Y., Machida, M., Akutsu, H., Uyama, T., Miyagawa, Y., et al. (2009). Mesenchymal to embryonic incomplete transition of human cells by chimeric OCT4/3 (POU5F1) with physiological co-activator EWS. Exp. Cell Res. *315*, 2727–2740.

Nagata, S., Toyoda, M., Yamaguchi, S., Hirano, K., Makino, H., Nishino, K., Miyagawa, Y., Okita, H., Kiyokawa, N., Nakagawa, M., et al. (2009). Efficient reprogramming of human and mouse primary extra-embryonic cells to pluripotent stem cells. Genes Cells *14*, 1395–1404.

Paku, S., Schnur, J., Nagy, P., and Thorgeirsson, S.S. (2001). Origin and structural evolution of the early proliferating oval cells in rat liver. Am. J. Pathol. *158*, 1313–1323.

Rodin, S., Domogatskaya, A., Ström, S., Hansson, E.M., Chien, K.R., Inzunza, J., Hovatta, O., and Tryggvason, K. (2010). Long-term self-renewal of human pluripotent stem cells on human recombinant laminin-511. Nat. Biotechnol. *28*, 611–615.

Schmelzer, E., Zhang, L., Bruce, A., Wauthier, E., Ludlow, J., Yao, H.L., Moss, N., Melhem, A., McClelland, R., Turner, W., et al. (2007). Human hepatic stem cells from fetal and postnatal donors. J. Exp. Med. *204*, 1973–1987.

Sumi, T., Tsuneyoshi, N., Nakatsuji, N., and Suemori, H. (2008). Defining early lineage specification of human embryonic stem cells by the orchestrated balance of canonical Wnt/beta-catenin, Activin/Nodal and BMP signaling. Development *135*, 2969–2979.

Takayama, K., Inamura, M., Kawabata, K., Tashiro, K., Katayama, K., Sakurai, F., Hayakawa, T., Furue, M.K., and Mizuguchi, H. (2011). Efficient and directive generation of two distinct endoderm lineages from human ESCs and iPSCs by differentiation stage-specific SOX17 transduction. PLoS ONE *6*, e21780.

Takayama, K., Inamura, M., Kawabata, K., Katayama, K., Higuchi, M., Tashiro, K., Nonaka, A., Sakurai, F., Hayakawa, T., Furue, M.K., and Mizuguchi, H. (2012a). Efficient generation of functional hepatocytes from human embryonic stem cells and induced pluripotent stem cells by HNF4α transduction. Mol. Ther. *20*, 127–137.

Takayama, K., Inamura, M., Kawabata, K., Sugawara, M., Kikuchi, K., Higuchi, M., Nagamoto, Y., Watanabe, H., Tashiro, K., Sakurai,

F., et al. (2012b). Generation of metabolically functioning hepatocytes from human pluripotent stem cells by FOXA2 and HNF1α transduction. J. Hepatol. *57*, 628–636.

Takayama, K., Kawabata, K., Nagamoto, Y., Kishimoto, K., Tashiro, K., Sakurai, F., Tachibana, M., Kanda, K., Hayakawa, T., Furue, M.K., and Mizuguchi, H. (2013). 3D spheroid culture of hESC/hiPSC-derived hepatocyte-like cells for drug toxicity testing. Biomaterials *34*, 1781–1789.

Tanimizu, N., Saito, H., Mostov, K., and Miyajima, A. (2004). Long-term culture of hepatic progenitors derived from mouse Dlk+ hepatoblasts. J. Cell Sci. *117*, 6425–6434.

Tashiro, K., Kawabata, K., Inamura, M., Takayama, K., Furukawa, N., Sakurai, F., Katayama, K., Hayakawa, T., Furue, M.K., and Mizuguchi, H. (2010). Adenovirus vector-mediated efficient transduction into human embryonic and induced pluripotent stem cells. Cell Reprogram. *12*, 501–507.

Tateno, C., Yoshizane, Y., Saito, N., Kataoka, M., Utoh, R., Yamasaki, C., Tachibana, A., Soeno, Y., Asahina, K., Hino, H., et al. (2004). Near completely humanized liver in mice shows human-type metabolic responses to drugs. Am. J. Pathol. *165*, 901–912.

Zhang, L., Theise, N., Chua, M., and Reid, L.M. (2008). The stem cell niche of human livers: symmetry between development and regeneration. Hepatology *48*, 1598–1607.

Zhao, D., Chen, S., Cai, J., Guo, Y., Song, Z., Che, J., Liu, C., Wu, C., Ding, M., and Deng, H. (2009). Derivation and characterization of hepatic progenitor cells from human embryonic stem cells. PLoS ONE *4*, e6468.

Knee Surg Sports Traumatol Arthrosc (2013) 21:736–739
DOI 10.1007/s00167-012-2078-3

KNEE

Change of signal intensity in the displaced medial meniscus after its reduction on MRI

Masayuki Hamada · Tomohiro Matsui · Kazutaka Kinugasa · Kenji Yoneda · Shuji Horibe · Konsei Shino

Received: 3 October 2011 / Accepted: 24 May 2012 / Published online: 9 June 2012

Abstract
Purpose To compare magnetic resonance (MR) signal intensity in the medial meniscus at the time of displacement and after its reduction in patients with a displaced bucket-handle tear of the meniscus associated with anterior cruciate ligament (ACL) injury.
Methods Nine chronic ACL-deficient patients (3 male, 6 female, mean age 29 years) with locking due to a displaced fragment of the medial meniscus following a bucket-handle tear were involved in this study. In all patients, the following two-stage surgeries were planned as follows: first operation, arthroscopic reduction of the meniscus; second operation, meniscal repair and ACL reconstruction after immobilization for 1–2 weeks. Magnetic resonance imaging (MRI) evaluation using coronal T2*-weighted images was performed when the knee was locked and after the meniscus was reduced. Signal intensity before and after meniscal reduction was compared in the same patients.
Results In 8 of the 9 patients, the displaced fragment exhibited high signal intensity in 1 patient and mildly high in 7 patients. After its reduction, the signal intensity changed to low in all 8 patients.
Conclusions A high-intensity signal in the displaced fragment of the medial meniscus may change to low after its reduction to its original position. Therefore, at the time of decision-making regarding meniscus repair for a displaced meniscus in a locked knee, surgeons should give priority to arthroscopic findings rather than to signal intensity on MRI.
Level of evidence Diagnostic study, Level III.

Keywords Medial meniscus · Bucket-handle tear · Knee MRI · Anterior cruciate ligament rupture · Meniscus reparability · Pitfalls in diagnosis

M. Hamada (✉) · T. Matsui · K. Kinugasa · K. Yoneda
Department of Orthopedic Sports Medicine, Hoshigaoka Kosei Nenkin Hospital, 4-8-1 Hoshigaoka Hirakata, Osaka 573-8511, Japan
e-mail: hamada-m@umin.ac.jp

S. Horibe
Faculty of Comprehensive Rehabilitation, Osaka Prefecture University, 3-7-30 Habikino, Osaka, Habikino 583-8555, Japan

K. Shino
Osaka Yukioka College of Health Science, 2-2-3 Ukita, Kita-ku, Osaka 530-0021, Japan

Introduction

Patients with chronic anterior cruciate ligament (ACL) deficiency may suffer from severe pain and loss of knee extension or locking due to a displaced fragment of the medial meniscus following bucket-handle tears. [8] Magnetic resonance imaging (MRI) is considered to be a useful tool for detecting displaced fragments in the notch. For example, 'absence of bow tie sign' or 'double posterior cruciate ligament sign' is a well-known MRI finding used to detect this pathology [4, 12, 13]. Recent studies have pointed out the usefulness of MRI for assessing the reparability of longitudinal or bucket-handle meniscal tears. In these reports, high signal intensity in the bucket-handle fragment was considered to indicate an irreparable meniscus. However, our preliminary observations indicate that most displaced menisci were evaluated as repairable at the time of arthroscopy, although MRI showed high signal intensity in their body [5, 7, 11]. This investigation was motivated by this discrepancy between the recent studies and our preliminary observations.

The aim of this study was to compare the magnetic resonance signal intensity of the meniscus at the time of displacement and after reduction in the same patients. The hypothesis was that displacement of the meniscus might affect the MR signal intensity.

Materials and methods

Our two-stage treatment strategy for patients with chronic ACL insufficiency associated with locked knee due to a bucket-handle tear of the medial meniscus was as follows: We first attempted to perform arthroscopy as soon as possible after presentation (within a few days). If the meniscus was considered irreparable, the torn fragment of the meniscus was excised, followed by the second stage of ACL reconstruction after regaining the full range of motion. However, if the meniscus was considered reparable, the displaced meniscus was reduced, followed by immobilization for 1–2 weeks with the knee kept in full extension. After the knee joint had regained the full range of motion, 4–6 weeks later, meniscus repair was performed in conjunction with ACL reconstruction [1].

During the period from 2002 to 2010, 23 patients with chronic ACL insufficiency visited our hospital complaining of pain and locked knee due to a bucket-handle tear of the medial meniscus. Of these patients, nine met the following inclusion criteria: (1) The meniscus was considered reparable at the time of the first operation, and it was reduced to its original position, (2) MRI evaluation was performed when the knee was locked due to the torn meniscus as well as when the meniscus was reduced.

Subjects comprised 3 male and 6 female patients with a mean age of 29 years (range, 16–44 years). The average time from ACL injury to knee locking was 10 months, ranging from 1 to 48 months. The average time from the knee locking to the first MRI examination was 4 days (range, 0–12 days), and that to the first operation was 9 days (range, 3–20 days). The average time from the first operation to the second MRI examination was 40 days (range, 13–68 days).

MR examination was performed with a 1.5-Tesla imager (Toshiba, Excelart Vantage). Coronal T2*-weighted images (TR, 555 ms; TE, 15 ms) were obtained. For all studies, a 16-cm field of view with a 192 × 400 matrix size was used. Slices were 4 mm in thickness with a gap of 0.8 mm. Signal intensity of the meniscus on MRI was assessed by 2 independent observers who were blinded to patients and between the observers until the completion of the data collection and, finally, were graded by the consensus of the observers [2, 6, 14].

MR signal intensity in the body of the displaced (or reduced) fragment was evaluated according to the following semi-quantitative criteria: It was graded as low when homogeneous normal low signal intensity was present, as mildly high when the signal intensity was greater than normal but less than that of adjacent joint fluid and as high when the signal intensity was equal to that of adjacent joint fluid [5, 7, 9, 11]. Interobserver reliability analysis by use of the κ statistic was performed regarding signal changes on MRI to determine the consistency between observers.

At arthroscopy, meniscus was considered as reparable when the tear was located in the outer third region, when the tear length was 1 cm or greater and when no major degeneration or fragmentation was observed in the meniscal body. In addition, if the patient was young and was eager to retain meniscus, meniscal repair was performed regardless of the tear location. In these 9 patients, all met the three criteria as mentioned above.

Results

κ values calculated for signal changes on MRI is 0.95. The value indicates almost perfect agreement between observers.

In 8 of the 9 patients, the first MRI examination showed that the displaced fragment exhibited high signal intensity in 1 patient and mildly high in 7 patients. As shown in Fig. 1, high signal intensity in the body of the meniscus was not linear but diffuse heterogenous one in all eight patients. The second MRI examination, after arthroscopic reduction of the meniscus to its normal position, showed that the high or mildly high signal intensity of the displaced fragment had changed to low in all 8 patients. However, in the remaining patient in whom the displaced fragment exhibited low intensity at first evaluation, signal intensity remained low after reduction. At the time of the second surgery, the meniscus was again judged as reparable in all 9 patients and was repaired in conjunction with ACL reconstruction.

Discussion

This study is the first to demonstrate that a high-intensity signal in the displaced fragment of a bucket-handle meniscal tear changes to low after reduction of the meniscus to its original position. High signal intensity in the body of the meniscus in MRI is a well-established criterion for diagnosing a meniscal tear or degeneration. Crues et al. have demonstrated that a linear high-intensity signal extending to the articular surface represents a tear and that an area of high intensity confined to the body of the meniscus represents intrameniscal degeneration. A review of the

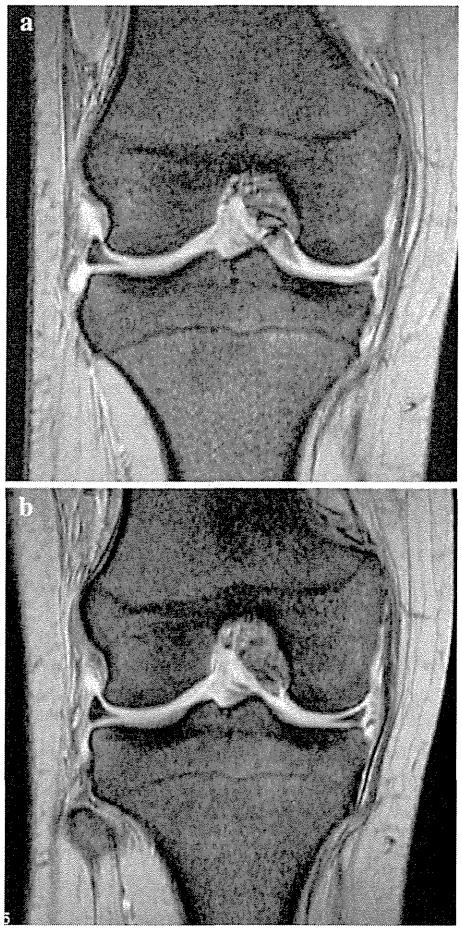

Fig. 1 MRI of a 22-year-old female patient **a** The displaced bucket-handle fragment showed mildly high signal intensity. **b** After reduction, the bucket-handle fragment showed low signal intensity

literature reveals that this method provides very good sensitivity and specificity for the diagnosis of lesions [3, 10]. However, from the results of this study, as far as the meniscus was displaced, high signal intensity does not always reflect the pathology of the meniscus correctly.

There are two possible explanations for this change in signal intensity. One could be that this high-intensity signal reflects only reversible or temporal oedema or inflammation due to displacement, as the MRI examinations were performed in the early phase after locking took place. The other could be the 'magic angle phenomenon', which is one of the artefacts inherent in MRI scanning. This phenomenon was recognized as the increase in signal intensity that occurs when collagen fibres in some tissues were oriented at 55°relative to the static magnetic field on short echo time MR images. It was observed in patellar tendon, ankle tendons and lateral meniscus. We speculated that, in this displaced medial meniscus, circumferential collagen fibres may twist and oriented at this specific angle relative to the static magnetic fields [9].

Because the meniscus plays an important functional role in the knee joint, repair of the meniscus is the best course of action to prevent degenerative changes after meniscectomy. In this sense, the preoperative prediction of meniscus reparability is a crucial issue. According to the recent studies evaluating the usefulness of MRI in assessing reparability of longitudinal or bucket-handle tears, fragments showing high signal intensity were considered irreparable [5, 7, 11]. Taking into account the signal intensity change observed between the reduced and displaced meniscus demonstrated in this study, however, we conclude that surgeons should give priority to arthroscopic findings rather than those of MRI at the time of decision-making regarding reparability of the displaced meniscus. In other words, it should be remembered that a heterogeneous image of the displaced meniscal fragment does not always indicate an irreparable meniscus, and this should be recognized as one of the pitfalls in interpreting meniscal pathology.

The small number of patients assessed is a limitation of this study. This is mainly due to the relatively low incidence of this pathology. In addition, MRI was performed only at the time of locking and not after reduction in most patients.

The other limitation of our study is the sequence of coronal MR images. In this series, only T2*-weighted images and proton density-weighted images, which have a short echo time, were used. Adding longer echo time sequence such as T2-weighted images may enable detection of a possible magic angle phenomenon and consequently improve the usefulness of MRI in assessing meniscus reparability.

Conclusion

High signal intensity in a displaced fragment of the medial meniscus on MRI may change to low after reduction to its original position. Therefore, caution should be exercised in the use of MRI when deciding on the reparability of the displaced meniscus.

References

1. Cannon WD Jr (1993) Problems of the menisci and their treatment, In: Larson RL, Grana WA eds The knee: form, function, pathology, and treatment. WB Saunders, Philadelphia pp. 429-469
2. Crema MD, Hunter DJ, Roemer FW, Li L, Marra MD, Nogueira-Barbosa MH, Le Graverand MP, Wyman BT, Guermazi A (2011) The relationship between prevalent medial meniscal intrasubstance signal changes and incident medial meniscal tears in

women over a 1-year period assessed with 3.0 T MRI. Skeletal Radiol 40:1017–1023
3. Crues JV 3rd, Mink J, Levy TL, Lotysch M, Stoller DW (1987) Meniscal tears of the knee: accuracy of MR imaging. Radiology 164:445–448
4. Helms CA, Laorr A, Cannon WD Jr (1998) The absent bow tie sign in bucket-handle tears of the menisci in the knee. Am J Roentgenol 170:57–61
5. Matsui T, Hamada M, Tagawa Y, Yoneda K, Miyama T, Kawai H (2010) Displaced bucket-handle tear of the medial meniscus—is MRI useful for predicting reparability? J Jpn Orthop Knee Arthrosc Sports Med. 35:556–559 (in Japanese)
6. Miao Y, Yu JK, Ao YF, Zheng ZZ, Gong X, Leung KK (2011) Diagnostic values of 3 methods for evaluating meniscal healing status after meniscal repair: comparison among second-look arthroscopy, clinical assessment, and magnetic resonance imaging. Am J Sports Med 39:735–742
7. Nourissat G, Beaufils P, Charrois O, Selmi TA, Thoreux P, Moyen B, Cassard X (2008) Magnetic resonance imaging as a tool to predict reparability of longitudinal full-thickness meniscus lesions. Knee Surg Sports Traumatol Arthrosc 16:482–486
8. O'Shea JJ, Shelbourne KD (2003) Repair of locked bucket-handle meniscal tears in knees with chronic anterior cruciate ligament deficiency. Am J Sports Med 31:216–220
9. Peterfy CG, Janzen DL, Tirman PF, van Dijke CF, Pollack M, Genant HK (1994) "Magic-angle" phenomenon: a cause of increased signal in the normal lateral meniscus on short-TE MR images of the knee. Am J Roentgenol 163:149–154
10. Stoller DW, Martin C, Crues JV 3rd, Kaplan L, Mink JH (1987) Meniscal tears: pathologic correlation with MR imaging. Radiology 163:731–735
11. Thoreux P, Réty F, Nourissat G, Rivière X, Safa P, Durand S, Masquelet AC (2006) Bucket-handle meniscal lesions: magnetic resonance imaging criteria for reparability. Arthroscopy 22:954–961
12. Watt AJ, Halliday T, Raby N (2000) The value of the absent bow tie sign in MRI of bucket-handle tears. Clin Radiol 55:622–626
13. Weiss KL, Morehouse HT, Levy IM (1991) Sagittal MR images of the knee: a low-signal band parallel to the posterior cruciate ligament caused by a displaced bucket-handle tear. Am J Roentgenol 156:117–119
14. Yoo WJ, Lee K, Moon HJ, Shin CH, Cho TJ, Choi IH, Cheon JE (2012) Meniscal morphologic changes on magnetic resonance imaging are associated with symptomatic discoid lateral meniscal tear in children. Arthroscopy 28:330–336

Clin Orthop Relat Res (2013) 471:1299–1304
DOI 10.1007/s11999-012-2707-7

Clinical Orthopaedics and Related Research®
A Publication of The Association of Bone and Joint Surgeons®

CLINICAL RESEARCH

The Intact Posterior Cruciate Ligament Not Only Controls Posterior Displacement but Also Maintains the Flexion Gap

Yoshio Matsui PhD, MD, Yoshinori Kadoya PhD, MD, Shuji Horibe PhD, MD

Received: 9 May 2012 / Accepted: 6 November 2012 / Published online: 21 November 2012

Abstract

Background The PCL is a strong stabilizer of the knee and provides posterior stability to the tibia. However, sagittal alignment of the PCL with the knee at 90° flexion suggests the PCL might play a role not only in posterior stabilization but also in maintaining the flexion gap.

Questions/purposes We determined whether the intact PCL helps maintain the flexion gap.

Methods We examined axial radiographs and gravity sag views of 17 patients with chronic isolated unilateral PCL injury. The flexion gap was defined as the mean value of the medial and lateral distances between the femoral and tibial bones on the axial radiograph. Increase in the flexion gap and posterior laxity were determined by comparing the patients' injured and contralateral uninjured knees.

Results The flexion gap of PCL injured knees (median, 7.5 mm; range, 5.3–11.5 mm; medial median, 6.2 mm; medial range, 3.7–8.3 mm; lateral median, 7.9 mm; lateral range, 5.3–11.5 mm) was larger than that seen in uninjured knees (median, 5.0 mm; range, 4.0–7.6 mm; medial median, 4.6 mm; medial range 3.4–7.1 mm; lateral median, 5.6; lateral range, 4.5–11.2 mm). The increment in the medial distance was similar to that in the lateral distance. Posterior laxity of injured knees was 9.1 (median); 5.4 to 15.2 (range) mm greater than that of uninjured knees. We found no correlation between posterior laxity and the flexion gap increment.

Conclusions Our data suggest the intact PCL controls posterior displacement and maintains the flexion gap.

Introduction

The PCL is a strong stabilizer of the knee and provides posterior stability to the tibia. However, sagittal alignment of the PCL with the knee at 90° flexion shows the PCL might play a role not only in posterior stabilization but also in maintaining the flexion gap (Fig. 1) [14]. The flexion gap is difficult to observe and few studies have investigated it in normal knees. Tokuhara et al. [21] observed the flexion gap (the distance between the femoral posterior condyles and the tibial boney surface) under valgus-varus stress by using MRI, and found the lateral flexion gap was larger than the medial flexion gap in normal knees. Although MRI enables three-dimensional observation of the knee at various flexion angles and under various forces, the procedure is time-consuming, costly, and can be painful

Each author certifies that he or she, or a member of his or her immediate family, has no funding or commercial associations (eg, consultancies, stock ownership, equity interest, patent/licensing arrangements, etc) that might pose a conflict of interest in connection with the submitted article.
All ICMJE Conflict of Interest Forms for authors and *Clinical Orthopaedics and Related Research* editors and board members are on file with the publication and can be viewed on request.
Each author certifies that his or her institution approved the human protocol for this investigation, that all investigations were conducted in conformity with ethical principles of research, and that informed consent for participation in the study was obtained.
This study was performed at Osaka Rosai Hospital, Sakai City, Osaka, Japan.

Y. Matsui (✉)
Osaka City General Hospital, 2-13-22, Miyakojima-hondori, Miyakojima-ku, Osaka City, Osaka 534-0021, Japan
e-mail: ichi23@js3.so-net.ne.jp

Y. Kadoya
Hannwa Arthroplasty Center, Sakai City, Osaka, Japan

S. Horibe
Osaka Prefecture University Graduate School of Comprehensive Rehabilitation, Habikino City, Osaka, Japan

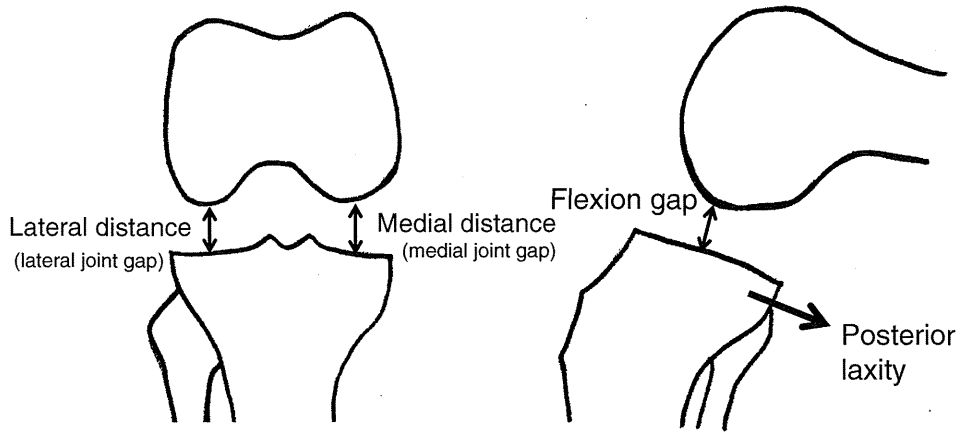

Fig. 1 Posterior laxity is sagittal laxity (how the tibia moves posteriorly from the femur). The flexion gap is the vertical distance between the femoral posterior condyle and the tibial plateau, and is the average of the medial and lateral distance.

for patients with knee pain. Kanekasu et al. [9] obtained plain radiographs with the x-ray beam projected along the femoral shaft (axial radiography) to evaluate the rotational position of the femoral component after TKA, and suggested this technique might be useful to evaluate the flexion gap. Similarly, Tokuhara et al. [20] reported axial radiography had similar accuracy to MRI in determining the flexion gap, and was useful in evaluating the flexion gap in normal knees.

Some studies [6, 7, 12, 23] have suggested the PCL plays a role in maintaining the flexion gap because the flexion gap increased after resection of the PCL in TKA. It is uncertain, however, whether the intact PCL maintains the flexion gap because the PCL is influenced by conditions such as arthritis and by anesthesia during TKA. Therefore, we sought to confirm whether the intact PCL maintains the flexion gap by using axial radiography.

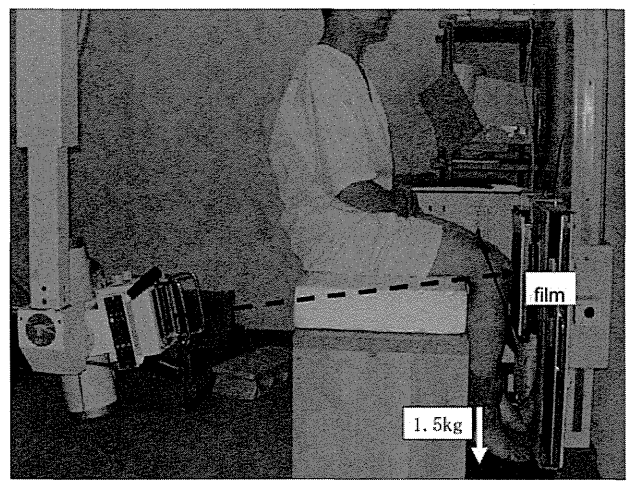

Fig. 2 Each patient was instructed to sit on the table with his or her lower legs hanging and to relax the thigh muscle. A 1.5-kg weight then was attached to the patient's ankle. The broken black arrow shows the path of the beam.

Patients and Methods

We retrospectively reviewed the radiographs of 17 patients (13 men, four women; mean age, 36 years; age range, 18–57 years) with isolated PCL injuries between March 2007 and May 2011. All patients reported having a sense of unclear knee instability in activities of daily living, despite receiving nonoperative medical treatment (eg, NSAIDs, physical therapy, braces). The time from injury to evaluation ranged from 3 months to 25 years. All patients had a positive traumatic history suggestive of PCL injury, and PCL tear was diagnosed by physical examination and confirmed by MRI and/or arthroscopy. The diagnosis was confirmed independently by three special sports orthopaedic surgeons (SH, YT, YY); if all three doctors came to the same conclusion, an isolated PCL injury was diagnosed. Thirteen of 17 patients had a posterior drawer Grade 2 PCL injury (6- to 10-mm posterior tibial translation) [2], whereas the other four patients had a Grade 3 injury (> 10-mm posterior tibial translation). We excluded patients with fracture, osteoarthritis, or other ligament lesions, such as those of the medial collateral ligament or posterolateral structures, with the use of multiple radiographs, MR images, and physical examinations. Regardless of the amount of posterior laxity, all 17 patients were scheduled for PCL reconstruction owing to their symptoms related to knee instability in activities of daily living.

The use of axial radiography, with the knee at 90° flexion and the x-ray beam projected along the femoral axis, has been reported in previous studies [3, 5, 9, 13, 20] (Fig. 2). This view can be used to evaluate the flexion gap and rotational position of the femoral component after TKA. The method for obtaining axial radiographs in our study was as follows: Each patient sat on a table with his or her lower legs hanging, and a 1.5-kg weight attached to the ankle (Fig. 2). The marker used to calculate radiograph

magnification (a 50-mm-diameter stainless steel disc) was attached to the lateral side of the knee. The patient was instructed to relax the leg muscles, especially the quadriceps. We explained the procedure, waited a few minutes until the patient was relaxed, and confirmed relaxation from clinical palpation of the thigh. We then obtained axial radiographs of the injured and contralateral uninjured knees to evaluate the increment of the flexion gap (Fig. 3).

All measurements were obtained at least twice by two observers (YM, YK). We measured the medial and lateral vertical distances from the midpoint of each condyle to the tibial boney surface on the axial radiograph; the flexion gap was expressed as the average of these distances (Fig. 4). Then, the increment of the flexion gap was determined by comparing the radiographs of the patients' injured and contralateral uninjured knees. We also evaluated posterior laxity on the gravity sag view [19]. The method for obtaining the gravity sag view was as follows (Fig. 5): The patient was placed supine with both hips flexed at 45° and both knees at 90° flexion. The x-ray beam was projected from the lateral side. Side-to-side differences of the tibia-femur step-off were measured as posterior shift, and posterior laxity was calculated as the amount of posterior shift in the injured knee minus that in the contralateral uninjured knee. We found interobserver and intraobserver variability in measuring the flexion gap on axial radiography to have intraclass correlation coefficients of 0.970 and 0.956, respectively.

Image data were transferred to a personal computer (Let's Note; Panasonic Corporation, Kadoma, Japan), and the flexion gap and posterior laxity were measured manually using an image analysis program (Vectorworks; A&A Co, Ltd, Tokyo, Japan). The program could change magnification, contrast, and brightness of the radiographs. We could manually detect the edges of measurement accurately by the program. The unit of measurement was 0.1 mm. Results were analyzed using StatView® 5.0 (SAS Institute Inc, Cary, NC, USA). Differences in instability between the injured and contralateral uninjured knees were analyzed by using the Wilcoxon signed-rank test, and Spearman's rank correlation coefficient test was used to analyze the correlation between the increment of the flexion gap and posterior laxity.

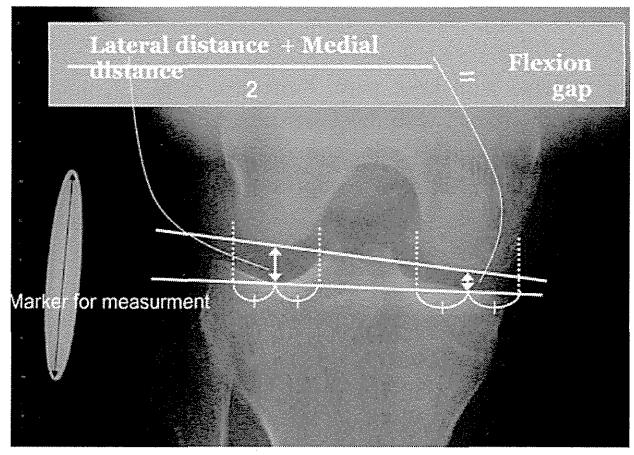

Fig. 4 We measured the medial and lateral vertical distances from the midpoint of each condyle to the tibial boney surface. Flexion laxity was expressed as the average of the medial and lateral distances.

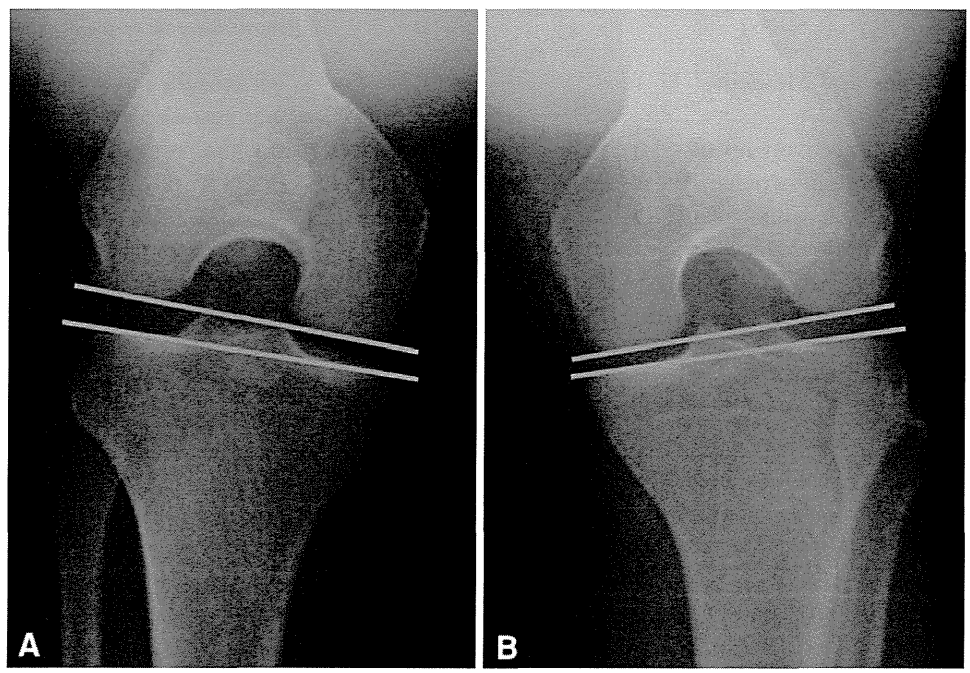

Fig. 3A–B Axial radiographs of (**A**) the PCL-injured knee and (**B**) the contralateral uninjured knee were used to evaluate the increment of the flexion gap. The magnification is the same because it was adjusted by using a 50-mm-diameter stainless steel disc as a marker.

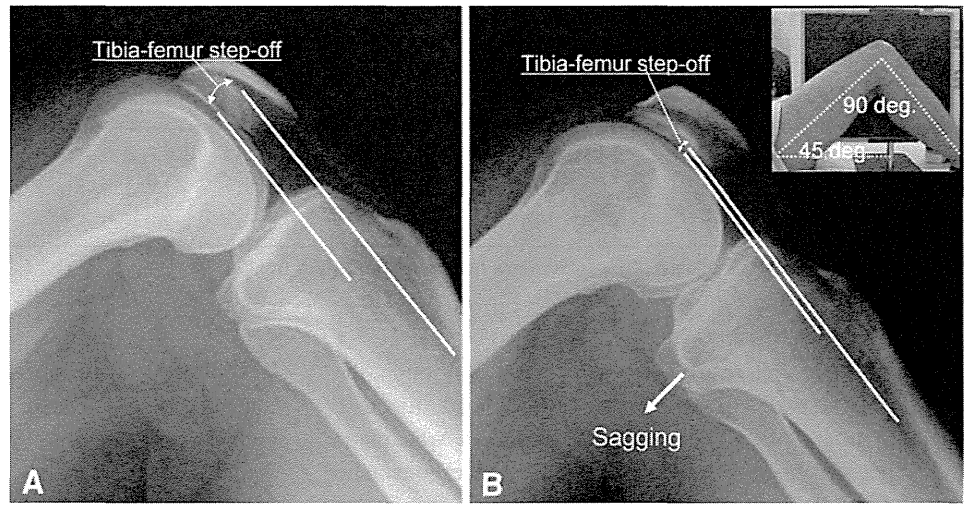

Fig. 5A–B Gravity sag views of (**A**) the contralateral uninjured knee and (**B**) the PCL-injured knee were taken in the supine position with both hips flexed at 45° and both knees at 90° flexion. Posterior shift is the side-to-side difference of the tibia-femur step-off.

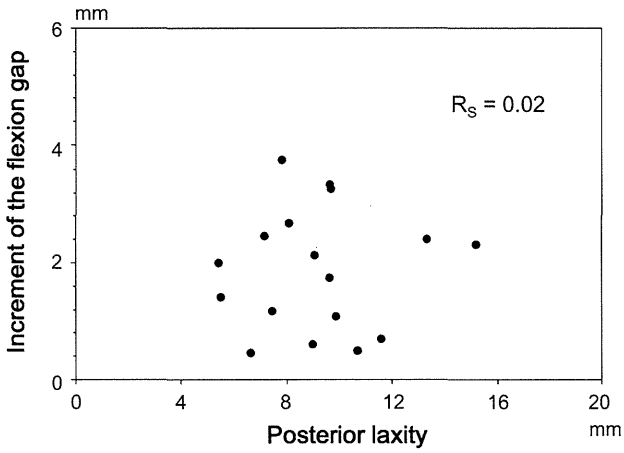

Fig. 6 A scatterplot shows the increment of posterior laxity versus the increment of the flexion gap. R_S is Spearman's rank correlation coefficient. No correlation was seen between the increment of posterior laxity and the increment of the flexion gap.

Results

The intact PCL appears to maintain the flexion gap: the flexion gap of the PCL-injured knees was greater ($p < 0.001$) than that of the uninjured knees. The median flexion gap of uninjured knees was 5.3 mm (range, 4.0–7.6 mm; medial median, 4.6 mm; medial range, 3.4–7.1 mm; lateral median, 5.6 mm; lateral range, 4.5–11.2 mm), whereas that of PCL-injured knees was 7.5 mm (range, 5.5–9.1 mm; medial median, 6.2 mm; medial range, 3.7–8.3 mm; lateral median, 7.9 mm; lateral range, 5.3–11.5 mm). The median flexion gap increment was 2.0 mm (range, 0.5–3.8 mm; medial median; 2.0 mm; medial range, 0.0–3.8 mm; lateral median, 2.3 mm; lateral range, −1.2 to 5.1 mm). We found no difference ($p = 0.543$) between the increment of the medial distance and that of the lateral distance. Median posterior laxity was 9.1 mm (range, 5.4–15.2 mm).

The increment of the flexion gap did not correlate with posterior laxity ($R_S = 0.02$; Fig. 6).

Discussion

With the knee at 90° flexion, the PCL is inclined 65° relative to the tibial plateau [14]; as such, there is the possibility the PCL plays a role not only in posterior stabilization but also in maintaining the flexion gap. It has been difficult to evaluate this possibility, however, because of the difficulty in observing the flexion gap. Tokuhara et al. [20] reported the flexion gap obtained from axial radiography correlated with that measured by MRI. Therefore, we used axial radiography to confirm whether the intact PCL maintains the flexion gap.

We acknowledge several limitations to our study. First, previous reports [3, 5, 9, 13, 20] have suggested contraction of the quadriceps could affect the flexion gap; therefore, it is essential that subjects have relaxed leg muscles during the examination. We explained this to each patient and waited a few minutes until the patients were relaxed before obtaining the radiographs. We also confirmed muscle relaxation with clinical palpation and facial expression. Second, prior researchers [3, 9, 13] have tested various loads on the ankle, and found the gap width was not directly proportional to the amount of distraction force. They concluded a 1.5-kg weight was suitable in terms of the subjects' comfort and the reproducibility of the results and that the interobserver and intraobserver variabilities in measuring the flexion gap on axial radiography were small. In the current study, we also found small interobserver and intraobserver variabilities in measuring the flexion gap on axial radiography. Third, the number of patients in our study was small; however, all the results showed that, compared with contralateral uninjured knees, PCL-injured knees had an increased flexion gap. There was no exception

Table 1. Summary of selective PCL resection studies

Study	Number of knees	Increment of flexion gap (mm)	
		Medial	Lateral
Kadoya et al. [7]	18 TKAs	4.8 ± 0.4*	4.5 ± 0.4*
Yagishita et al. [23]	30 TKAs	2.7 ± 0.7*	2.9 ± 2.2*
Current study	17 PCL injuries	2.0 (0.0–3.8)#	2.3 (−1.2 to 5.1)#

* Values are expressed as mean ± SD; #values are expressed as median (range).

in the results. The result was reliable, even though the sample was small. Fourth, it was difficult to diagnose chronic isolated PCL injuries. The diagnosis was made independently by three sports orthopaedic surgeons who each had more than 10 years of experience. Each surgeon had to come to the same conclusion to diagnose a chronic isolated PCL injury. Four patients had a Grade 3 injury and some researchers [11, 17] have reported one should be suspicious for other ligament injuries in patients with Grade 3 injuries. However, the four patients in our study were diagnosed with an isolated PCL injury based on a thorough medical examination. Even if these four patients were excluded, the flexion gaps of the remaining 13 patients' PCL-injured knees increased, and the results would be the same.

Our data suggest the intact PCL not only controls posterior displacement but also maintains the flexion gap. Compared with the contralateral uninjured knees, all PCL-injured knees had an increased flexion gap. Some studies [7, 23] have reported PCL resection in TKA increases the flexion gap (Table 1); however, those researchers used intraoperative measurements and knees with osteoarthritis or rheumatoid arthritis. The intraoperative measurements might have been influenced by anesthesia, the incision, and/or release of the capsule. Our patients had one normal knee and one with isolated PCL injury, and our observations suggested the PCL in the normal knees played a role in maintaining the flexion gap.

Other factors reportedly influence flexion laxity. Saeki et al. [16] and Yagishita et al. [23] reported that selective medial collateral ligament release in TKA increases the flexion gap by using an intraoperative measurement. Furthermore, selective lateral collateral ligament release or popliteus tendon release increased the flexion gap in one cadaver study [8]. With the knee at 90° flexion, the patella tendon was inclined 90° relative to the tibial plateau in one MRI study [10]. Owing to these factors, we believe that compared with posterior laxity, the flexion gap increment in PCL-injured knees is small. The average flexion gap increment was slightly smaller than that in TKA [7, 23] (Table 1). The small differences might be related to the influence of anesthesia, incisions, and/or capsular release.

Regardless of the amount of posterior laxity, all patients were scheduled for PCL reconstruction owing to the symptoms related to knee instability. The surgical indication for chronic isolated PCL injury remains controversial [11]. Many reports [1, 4, 15, 18, 22] have noted athletes with PCL deficiencies function well despite obvious posterior laxities, while some studies [15, 18, 22] have indicated there is no correlation between the amount of posterior laxity and clinical knee function. Surgical decision making is difficult and based on many factors. In addition to our results, if it is clarified that an increase in the flexion gap influences the clinical results of PCL reconstruction, the flexion gap increase could be a factor to help clinicians choose a surgical intervention for treatment of PCL injuries.

Our observations suggest the intact PCL functions not only as a posterior stabilizer of the tibia but also maintains the flexion gap in normal knees.

Acknowledgments We thank Y. Tanaka PhD, MD, and Y. Yonetani PhD, MD, for gathering data and helping to diagnose chronic isolated PCL injuries.

References

1. Bach BR Jr. Graft selection for posterior cruciate ligament surgery. *Oper Tech Sports Med.* 1993;1:104–109.
2. Baumfeld J, Dahm DL. Current concept in posterior cruciate ligament reconstruction. In: Scott WN, eds. *Insall & Scott Surgery of the Knee.* 4th ed. Philadelphia, PA: Churchill Livingstone; 2006.737–745.
3. Fujii T, Kondo M, Tomari K, Kadoya Y, Tanaka Y. Posterior condylar cartilage may distort rotational alignment of the femoral component based on posterior condylar axis in total knee arthroplasty. *Surg Radiol Anat.* 2012;34:633–638.
4. Harner CD, Hoher J. Evaluation and treatment of posterior cruciate ligament injuries. *Am J Sports Med.* 1998;26:471–482.
5. Hatayama K, Terauchi M, Higuchi H, Yanagisawa S, Saito K, Takagishi K. Relationship between femoral component rotation and total knee flexion gap balance on modified axial radiographs. *J Arthroplasty.* 2011;26:649–653.
6. Heesterbeek P, Keijsers N, Jacobs W, Verdonschot N, Wymenga A. Posterior cruciate ligament affects antero-posterior translation during flexion gap distraction in total knee replacement: an intraoperative study involving 50 patients. *Acta Orthop.* 2010;81:471–477.

7. Kadoya Y, Kobayashi A, Komatsu T, Nakagawa S, Yamano Y. Effects of posterior cruciate ligament resection on the tibiofemoral joint gap. *Clin Orthop Relat Res.* 2001;391:210–217.
8. Kanamiya T, Whiteside LA, Nakamura T, Mihalko WM, Steiger J, Naito M. Ranawat Award paper: Effect of selective lateral ligament release on stability in knee arthroplasty. *Clin Orthop Relat Res.* 2002;404:24–31.
9. Kanekasu K, Kondo M, Kadoya Y. Axial radiography of the distal femur to assess rotational alignment in total knee arthroplasty. *Clin Orthop Relat Res.* 2005;434:193–197.
10. Komatsu T, Kadoya Y, Nakagawa S, Yoshida G, Takaoka K. Movement of the posterior cruciate ligament during knee flexion: MRI analysis. *J Orthop Res.* 2005;23:334–339.
11. Lee BK, Nam SW. Rupture of posterior cruciate ligament: diagnosis and treatment principles. *Knee Surg Relat Res.* 2011;23:135–141.
12. Mihalko WM, Miller C, Krackow KA. Total knee arthroplasty ligament balancing and gap kinematics with posterior cruciate ligament retention and sacrifice. *Am J Orthop (Belle Mead NJ).* 2000;29:610–616.
13. Nagamine R, Kondo K, Nomura H, Kanekasu K, Sonohata M, Sugioka Y. Shape of the joint gap for 90° and 120° knee flexion after total knee arthroplasty. *J Orthop Sci.* 2008;13:354–358.
14. Nakagawa S, Johal P, Pinskerova V, Komatsu T, Sosna A, Williams A, Freeman MA. The posterior cruciate ligament during flexion of the normal knee. *J Bone Joint Surg Br.* 2004;86:450–456.
15. Parolie JM, Bergfeld JA. Long-term results of nonoperative treatment of isolated posterior cruciate ligament injuries in the athlete. *Am J Sports Med.* 1986;14:35–38.
16. Saeki K, Mihalko WM, Patel V, Conway J, Naito M, Thrum H, Vandenneuker H, Whiteside LA. Stability after medial collateral ligament release in total knee arthroplasty. *Clin Orthop Relat Res.* 2001;392:184–189.
17. Sekiya JK, Whiddon DR, Zehms CT, Miller MD. A clinically relevant assessment of posterior cruciate ligament and posterolateral corner injuries: evaluation of isolated and combined deficiency. *J Bone Joint Surg Am.* 2008;90:1621–1627.
18. Shelbourne KD, Davis TJ, Patel DV. The natural history of acute, isolated, nonoperatively treated posterior cruciate ligament injuries: a prospective study. *Am J Sports Med.* 1999; 27:276–283.
19. Shino K, Mitsuoka T, Horibe S, Hamada M, Nakata K, Nakamura N. The gravity sag view: a simple radiographic technique to show posterior laxity of the knee. *Arthroscopy.* 2000;16:670–672.
20. Tokuhara Y, Kadoya Y, Kanekasu K, Kondo M, Kobayashi A, Takaoka K. Evaluation of the flexion gap by axial radiography of the distal femur. *J Bone Joint Surg Br.* 2006;88: 1327–1330.
21. Tokuhara Y, Kadoya Y, Nakagawa S, Kobayashi A, Takaoka K. The flexion gap in normal knees: an MRI study. *J Bone Joint Surg Br.* 2004;86:1133–1136.
22. Torg JS, Barton TM, Pavlov H, Stine R. Natural history of the posterior cruciate ligament-deficient knee. *Clin Orthop Relat Res.* 1989;246:208–216.
23. Yagishita K, Muneta T, Ikeda H. Step-by-step measurements of soft tissue balancing during total knee arthroplasty for patients with varus knees. *J Arthroplasty.* 2003;18:313320.

Knee Surg Sports Traumatol Arthrosc
DOI 10.1007/s00167-013-2557-1

KNEE

MRI analysis of single-, double-, and triple-bundle anterior cruciate ligament grafts

Yoshinari Tanaka · Yasukazu Yonetani · Yoshiki Shiozaki · Takashi Kanamoto · Keisuke Kita · Hiroshi Amano · Masashi Kusano · Masashi Hirakawa · Shuji Horibe

Received: 26 October 2012 / Accepted: 29 May 2013

Abstract
Purpose The purpose of the study was to evaluate the entire course of ACL grafts on coronal oblique MR images, focusing on differences in graft morphology and graft-to-tunnel healing among single-bundle (SB), double-bundle (DB), and triple-bundle (TB) reconstructions.
Methods Eighty-three patients underwent anatomical ACL reconstruction using the semitendinosus tendon. SB reconstruction was performed on 20 patients, DB on 29 patients, and TB on 34 patients. The anteromedial-bundle (AMB) and posterolateral-bundle (PLB) images were extracted from coronal oblique images of grafts at 6 months to visualize their entire course. Signal intensity of grafts was measured independently in three regions: (1) intra-femoral tunnel region, (2) intra-articular region, and (3) intra-tibial tunnel region, followed by calculation of the signal-to-noise quotient (SNQ). To evaluate graft-to-tunnel healing, T2-weighted images were examined for the presence of a high signal-intensity lesion between the graft and bone tunnel around the tunnel aperture.
Results AMB images showed that SB graft was thick throughout the entire course, while DB graft was thinner than SB graft. TB graft showed a fan shape approaching the tibial tunnels. The SNQ in the femoral tunnel of SB graft was significantly lower than in the DB and TB grafts. High signal-intensity lesions were frequently observed around the femoral tunnel aperture in PLB images of DB and TB grafts compared to SB grafts.
Conclusion Gross morphology of TB grafts resembled that of the natural ACL. However, the graft-to-tunnel healing around the femoral tunnel seemed to be insufficient in PLB images of DB and TB compared to SB grafts.
Level of evidence III.

Keywords ACL graft · Coronal oblique MRI · Multiple bundle reconstruction · Tendon-to-bone healing

Y. Tanaka (✉) · T. Kanamoto · K. Kita · H. Amano
Department of Sports Orthopedics, Osaka Rosai Hospital, 1179-3 Nagasone-cho, Kita-ku, Sakai, Osaka 583-8555, Japan
e-mail: yoshi-tanaka@iris.eonet.ne.jp

Y. Yonetani
Department of Orthopedic Surgery, Osaka University Graduate School of Medicine, Osaka University, Osaka, Japan

Y. Shiozaki · M. Kusano
Department of Orthopedic Surgery, Seifu Hospital, Sakai, Japan

M. Hirakawa
Department of Orthopedic Surgery, Oita University, Oita, Japan

S. Horibe
Faculty of Comprehensive Rehabilitation, Osaka Prefecture University, Habikino, Osaka, Japan

Introduction

Anterior cruciate ligament (ACL) reconstruction using hamstring tendon has become popular because of low donor site morbidity [9, 10, 19]. Recent improvements in operative procedures have made it possible to perform anatomical single-, double-, and triple-bundle ACL reconstruction [13, 31, 40]. Anatomical ACL reconstruction offers superior biomechanical performance [17, 39] and clinical outcome [21] compared to the traditional Rosenberg's one or two femoral socket ("bi-socket") procedure, for which results remain controversial [28, 30].

Recent anatomical studies have provided useful information about the ACL footprint and its surrounding anatomical landmarks [7, 12, 14, 26, 29] that enable surgeons

Published online: 09 June 2013

Table 1 Patients' demographics

	1B	2B	3B
Total number of patients	20	29	34
Age at the time of surgery (range)	38.2 (15–52)	23.3 (13–46)	24.2 (15–51)
Gender (male/female)	9: 11	12: 17	27: 7
Preoperative period (months)	62.4	22.4	6.7
IKDC activity level			
Level 1-2	7	15	28
Level 3-4	13	14	6
Lachman test[a]			
Normal	19	27	33
1+	1	2	1
2+	0	0	0
Pivot shift test[a]			
Normal	20	23	32
1+	0	6	2
2+	0	0	0
KT-2000 side-to-side difference (mm)[a]	0.5 ± 0.9	1.3 ± 1.6	0.6 ± 1.5

[a] The results of Lachman test, pivot shift test, and KT-2000 were assessed at 6 months postoperatively

to perform accurate and reproducible reconstruction, probably leading to recognition of the advantages of multiple bundle reconstructions. However, results of second-look arthroscopy after double- and triple-bundle reconstructions show poor morphological status around the femoral tunnel aperture of the posterolateral grafts [2, 25, 34]. Otsubo et al., reported substantial damage in 11 % of posterolateral grafts and Ahn et al., showed complete tear or obvious elongation in 16 % of posterolateral grafts.

The damage in posterolateral grafts may be due to a biological healing process that includes graft remodeling and graft-to-tunnel healing [3, 5, 27]. To understand the status of the graft as a whole, it is essential to evaluate both the graft itself and the relationship between the graft and the bone tunnel. Magnetic resonance imaging (MRI) is useful for assessment of normal, injured, and reconstructed ACLs [8, 11, 16, 33, 41]. In addition, several studies examining the biological healing process of transplanted grafts using sagittal oblique MR images, with or without contrast enhancement, showed that maximum vascular response occurred at approximately 24 weeks postoperatively [4, 22, 24]. However, sagittal oblique images could not fully visualize the intra-femoral tunnel. Coronal oblique MRI scans can visualize the entire course of the ACL in vivo [33, 34] and also enable assessment of the integrity of individual ACL bundles in double-bundle reconstruction [6]. Furthermore, coronal oblique images are predicted to be useful for simultaneous evaluation of the intra-femoral tunnel region and the intra-tibial tunnel region, which has never been performed so far.

The purpose of the present study was to evaluate gross morphology of the anteromedial and posterolateral portions of single-, double-, and triple-bundle ACL grafts at 6 months postoperatively using coronal oblique MR images in addition to traditional sagittal oblique images. In addition, both the intra-articular and the intra-tunnel regions of the grafts were also examined to understand graft status and graft-to-tunnel healing. It was hypothesized that coronal oblique MR images would make it possible to evaluate the intra-tunnel region of the ACL grafts as well as the intra-articular region.

Materials and methods

Of 431 patients who underwent ACL reconstruction in our hospital between 2008 and 2010, 83 patients provided informed consent for MRI analysis of their ACL grafts. The median age of the 48 male participants and 35 female participants was 24.0 years (range 13–52 years). The patients underwent one of the following three operative procedures based on age and activity level: single-bundle ACL reconstruction (SB; 20 patients), double-bundle reconstruction (DB; 29 patients), and triple-bundle reconstruction (TB; 34 patients). The median follow-up duration was 22.7 months (range 6.0–50.7). Patient demographics are summarized in Table 1. Those who underwent SB-ACL reconstruction were relatively old and inactive, while patients who had DB or TB reconstructions were relatively young and active.

Surgical procedures for single-, double-, and triple-bundle reconstruction

The anatomical SB-, DB-, and TB-ACL reconstructions have been performed as previously described [1, 13, 25, 32].

SB-ACL reconstruction (Fig. 1a, d)

The quadrupled SB graft was 60–70 mm in length and 7–9 mm in diameter. After identification of the femoral and tibial ACL footprints, a femoral socket was created between the Resident's ridge and the posterior margin of the notch at the 2:30 position for the left or 9:30 for the right knee to a depth of 22–25 mm using a drill bit of appropriate (7–9 mm) diameter, followed by penetration with an Endobutton-drill to the lateral femoral cortex. The tibial tunnel was created into the center of the footprint using the Director tibial guide (Smith & Nephew

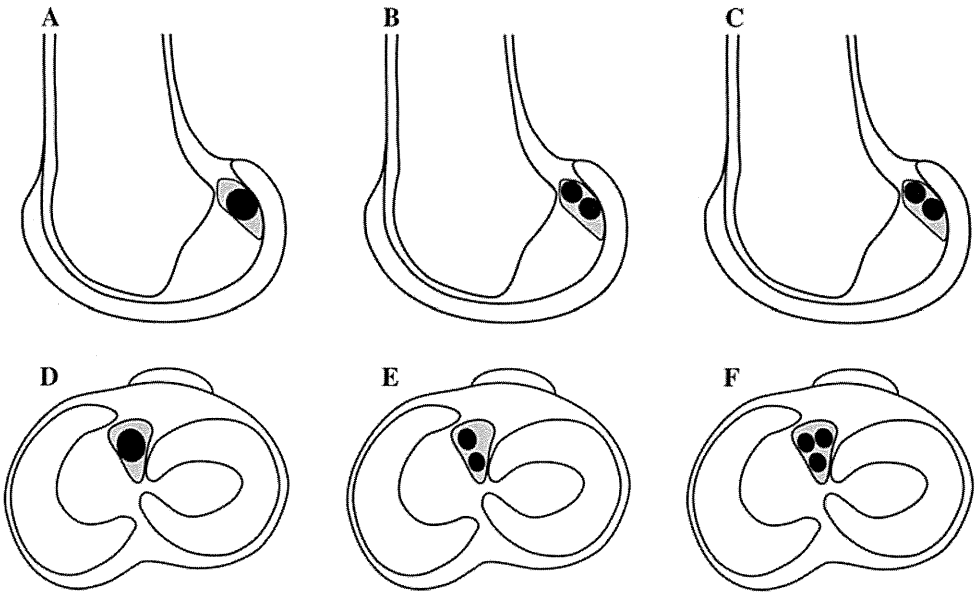

Fig. 1 Tunnel locations in the ACL footprints. **a–c** Femoral tunnels. **d–f** Tibial tunnels. **a**, **d** SB reconstruction. **b**, **e** DB reconstruction. **c**, **f** TB reconstruction

Endoscopy, Andover, MA, USA) and the cannulated drill. Endobutton CL was used for femoral fixation and a double-spike plate (DSP; MEIRA Corp., Nagoya, Japan) for tibial fixation [31]. The graft was fixed to the tibia at 15°–20° flexion under initial tension of 30N.

DB-ACL reconstruction (Fig. 1b, e)

Two double-looped anteromedial (AM) and posterolateral (PL) grafts, which were 60–70 mm in length and 5–6 mm in diameter, were prepared. Two femoral tunnels were created between the Resident's ridge and the posterior margin of the notch at 2:00 and 3:00 for the left or at 9:00 and 10:00 for the right knee using the anterolateral entry femoral aimer (Smith & Nephew Endoscopy, Andover, MA, USA). Two tibial tunnels were created within the footprint with the tibial guide and a drill bit of appropriate diameter (5–6 mm). After the AM and PL grafts were fixed with Endobutton CLs to the femur, each graft was fixed to the tibia at 15°–20° flexion under initial tension of 15N.

TB-ACL reconstruction (Fig. 1c, f)

TB grafts were prepared by transacting the tendon in half to make double-looped anteromedial/intermediate (AM/IM) and PL grafts, and attaching an Endobutton CL to the loop. However, the AM/IM graft was left to be bifurcated while the PL graft was tied with a suture. Two femoral tunnels were created as described in the DB procedure. For the tibia, three tibial tunnels were made using the tibial guide, the offset parallel pin guide (Smith & Nephew Endoscopy, MA, USA), and a drill bit of appropriate diameter (5–6 mm). After fixation of the AM/IM and PL grafts with Endobutton CLs to the femur, each graft was fixed to the tibia at 15°–20° flexion using two double-spike plates (DSPs) with an initial tension of 15N.

MRI images of ACL grafts

The sagittal oblique and coronal oblique images of the ACL were obtained as previously described [33, 34]. Briefly, all patients were examined with the knee in an actively extended position using a 0.4T MRI scanner (Hitachi, Tokyo, Japan): fast spin-echo T2-weighted images (T2WI; TR/TE 3000/90) were obtained in the sagittal oblique and coronal oblique planes with 3-mm slice thickness and 1-mm slice spacing [34]. The coronal oblique imaging plane was defined parallel to the Blumensaat's line (Fig. 2a). The AMB and the PLB images were identified as the most anterior and posterior slices of the ACL graft, respectively, from coronal oblique images (Fig. 2b, c).

MRI evaluation of transplanted ACL grafts

The grafts from the oblique coronal MRI images were evaluated at 6 months postoperatively, focusing on gross morphology, signal intensity of the grafts, and bone-to-graft healing around the bone tunnel aperture. Increased signal intensity of the graft has been described within a year postoperatively, and to understand a change within the graft, its signal intensity was measured independently for three regions in the coronal oblique images: (1) the intra-femoral tunnel region, (2) the intra-articular region, and (3) the intra-tibial tunnel region of the grafts (Fig. 3). The measurements were performed for the AMB and PLB images, and the signal/noise quotient (SNQ) was calculated, with SNQ = [signal (specific site of the

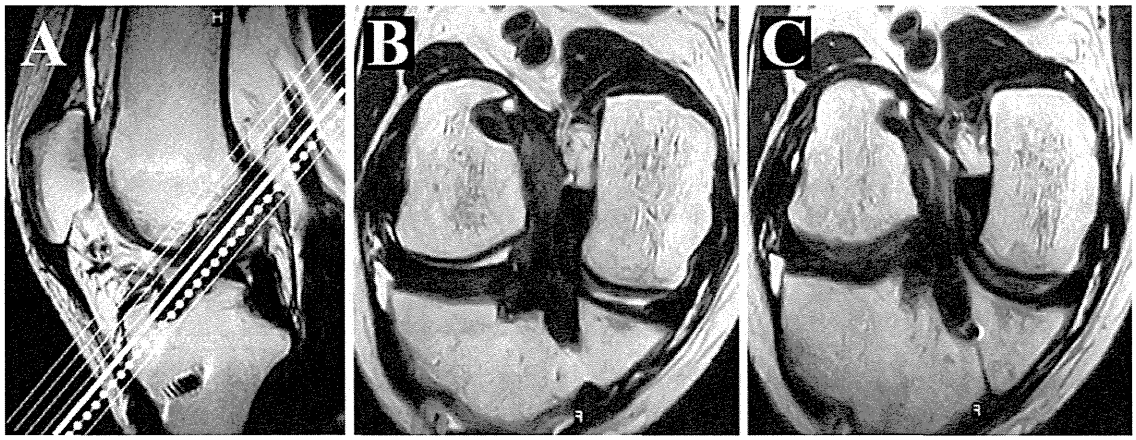

Fig. 2 Coronal oblique images of the ACL graft. **a** Scout view: slices corresponding to the AMB (*solid line*) and PLB (*dotted line*) images. Representative coronal oblique AMB (**b**) and PLB (**c**) images

graft) −signal (PCL)]/signal (background) [37]. Circular 5-mm diameter regions of interest (ROI) were evaluated for measuring signal of the PCL and background. The background ROI was placed approximately 1 cm medial and 2 cm distal to the medial joint line. Additionally, intra-observer and inter-observer agreement for signal intensity were evaluated using kappa correlation coefficient with 95 % confidence interval (CI). As for inter-observer agreement, signal intensity within the ROI of the intra-articular region of the AMB in 20 cases was examined independently by two reviewers. Similarly, signal intensity of the same portion was measured twice by one of the observers with an interval of 1 week between measurements and intra-observer agreement was evaluated. The analysis was performed using SPSS for Windows software (SPSS Inc., Chicago, IL, USA). In terms of graft-to-tunnel healing, previous studies by 2nd-look arthroscopy revealed poor results around the femoral tunnel aperture in the PLB compared to AMB [2, 25, 35]. Additionally, T2-weighted images in our pilot study had showed a high signal-intensity lesion between the graft and the tunnel wall in some cases. Therefore, to evaluate graft-to-bone tunnel healing, T2-weighted images were examined for the presence of a high signal-intensity lesion between the graft and tunnel wall around the femoral and tibial tunnel apertures (Fig. 3).

In addition, to evaluate the ACL graft in another direction, sagittal obliquity of the graft was examined on sagittal oblique images using the ACL angle, which was defined by the intersection of two lines: one tangential to the anterior aspect of the mid portion of the ACL and the other tangential to the anterior aspect of the intercondylar eminence [20]. Furthermore, the contralateral native ACL could be simultaneously evaluated with MRI in 78 cases, and the ACL angle was compared between the graft and native ACL.

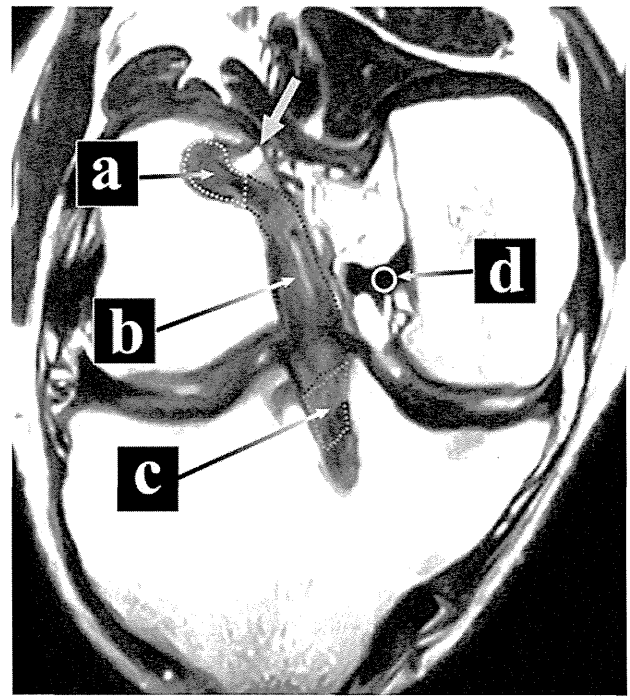

Fig. 3 Measurement of signal intensity in three regions of the ACL graft and the PCL: (*a*) intra-femoral tunnel region surrounded by a *yellow-dotted line*, (*b*) intra-articular region surrounded by a *red-dotted line*, (*c*) intra-tibial tunnel region surrounded by a *sky blue-dotted line*, and (*d*) the PCL. The background ROI was approximately 1 cm medial and 2 cm distal to the medial joint line (not shown). A high signal-intensity lesion between the graft and femoral tunnel wall is shown with a *yellow arrow*

Statistical analysis

Data were analyzed using SPSS for Windows software (SPSS Inc., Chicago, IL, USA). The Student's *t* test and Mann–Whitney U test were used to assess differences among the three operative procedures regarding SNQ values, ACL angle, and incidence of high signal-intensity

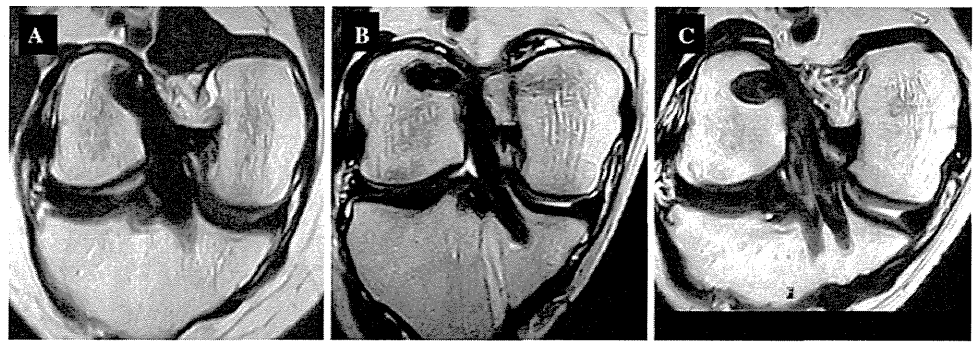

Fig. 4 Representative coronal oblique AMB images of SB (**a**), DB (**b**), and TB (**c**) reconstructions

lesions between the graft and tunnel wall. Correlation between MRI findings and clinical results was examined using the chi-square test and the Mann–Whitney *U* test. The level of significance was set at $P < 0.05$.

Results

Gross morphology of single-, double-, and triple-bundle ACL grafts

The AMB images showed that the SB graft had an approximately equal thickness over its entire course, while the DB graft was thinner than the SB graft (Fig. 4a, b). The TB graft had a fan shape approaching the tibial tunnels as preoperatively planned to mimic morphology of the native ACL (Fig. 4c). On the other hand, PLB images showed no apparent difference in morphology among the three graft procedures. As for tunnel placement, all of the tibial tunnels of the AMB were settled in the slope of the medial intercondylar ridge where the native ACL attaches [34]. On the other hand, two PLB grafts (2.4 %) attached to the base of the medial intercondylar ridge, indicating relatively non-anatomical tunnel placement in two cases. One was the PLB of the DB and the other was the TB one. Femoral tunnel placement, especially the relationship between the femoral tunnel and the Resident's ridge, could not be precisely evaluated because the ridge was too small to be identified on postoperative MR images. As for sagittal obliquity, mean ACL angles of the SB, DB, and TB grafts in the sagittal oblique images were 50.2° ± 4.9°, 49.8° ± 3.7°, and 47.8° ± 4.0°, respectively. These values were not significantly different when compared to the contralateral native ACL (mean 52.1° ± 3.8°).

Signal intensity of the grafts

The intra-observer and inter-observer agreement for the signal intensity of the ROI, as assessed by the kappa coefficient, was excellent (0.97: CI 0.93–0.99 and 0.97: CI 0.93–0.99, respectively). The SNQ values of the grafts were summarized in Table 2.

Intra-articular region

AMB and PLB images showed no significant difference in mean SNQ values of the SB, DB, and TB grafts.

Intra-femoral tunnel region

AMB images showed a significant difference in mean SNQ in SB, DB, and TB grafts. Similarly, PLB images showed a significantly lower mean SNQ value in SB compared to DB and TB grafts.

Intra-tibial tunnel region

There were no statistically significant differences among mean SNQ values of the SB, DB, and TB grafts.

Bone-to-graft healing in the femoral tunnel

With regard to bone-to-graft healing, two characteristic lesions were found around the bone tunnels. One was an intra-tunnel lesion with high signal intensity around the femoral tunnel aperture located superoposterior to the graft (Fig. 3), and the other was a bony cyst previously described [36]. The incidence of these lesions is summarized in Tables 3 and 4. The incidence of high signal-intensity lesions was significantly higher in PLB images than in AMB images regardless of operative method, although there was no difference among the procedures. Additionally, the lesion occurred less frequently in the AMB of SB grafts compared to the other procedures. However, these high signal-intensity lesions around the grafts were observed on the tibial side in only four cases. The bony cyst around the graft tended to localize around the tibial tunnels, although the overall incidence was low compared to that of the high signal-intensity lesions (Table 4).

Correlation between MRI findings and clinical results

The results of Lachman test and positive pivot shift test were described in Table 1. The results of the current MRI study, which included the SNQ of the grafts and the

Table 2 Graft signal-to-noise quotients (SNQ)

	SB	DB	TB
Intra-articular region			
AMB	4.8 ± 2.2	5.5 ± 2.3	4.2 ± 1.3
PLB	4.4 ± 2.7	5.3 ± 2.6	4.9 ± 1.6
Intra-femoral tunnel region			
AMB	2.5 ± 2.1	4.8 ± 3.8*	4.2 ± 1.8*
PLB	3.1 ± 3.0	4.6 ± 2.8*	4.8 ± 2.5*
Intra-tibial tunnel region			
AMB	3.8 ± 2.2	3.8 ± 2.6	3.4 ± 1.4
PLB	3.2 ± 2.2	4.6 ± 3.6	4.0 ± 1.9

The SNQ values of the SB were significantly higher compared to those of the DB and TB (* $P < 0.05$)

Table 3 Incidence of high signal-intensity lesions between the graft and the tunnel

	Femoral tunnel (%)		Tibial tunnel (%)	
	AM	PL	AM	PL
SB	1 (5.0)	6 (30.0)	1 (5.0)	0 (0.0)
DB	8 (27.6)	19 (55.2)	1 (3.4)	1 (3.4)
TB	4 (11.8)	15 (44.1)	0 (0.0)	1 (2.9)

Table 4 Incidence of bony cyst around the graft

	Femoral tunnel (%)	Tibial tunnel (%)
SB	0 (0.0)	4 (20.0)
DB	2 (6.9)	5 (17.2)
TB	0 (0.0)	2 (5.9)

presence of the high signal-intensity lesions around the femoral tunnel aperture, did not make significant differences in the results of Lachman test and pivot shift test.

Discussion

The first research question addressed whether coronal oblique MR images enable to evaluate the entire course of the ACL graft. The current results revealed that coronal oblique MR images made it possible to evaluate the intra-tunnel region of the grafts as well as the intra-articular region. As previously described, coronal oblique MRI scans can visualize the entire course of the ACL in vivo [33, 34] and also enable assessment of the integrity of individual ACL bundles in DB reconstruction [6]. In addition to these advantages, our results revealed that coronal oblique images can clarify the relationship between the graft and the femoral tunnel because anatomically placed femoral tunnels, which are located at the inner side of the lateral femoral condyle, are not suitable for assessment with sagittal oblique images.

The second research question addressed whether coronal oblique images show differences in the graft morphology and the graft-to-tunnel healing among the three operative procedures. As for graft morphology, sagittal oblique images revealed that anatomically placed grafts had the same obliquity as seen in native ACLs, regardless of differences in surgical procedure. However, coronal oblique scans visualized differences in graft morphology among the three reconstruction procedures. Graft morphology in AMB images differed among the three reconstruction techniques as predicted preoperatively: SB grafts were thick in the mediolateral direction throughout the entire course compared to DB grafts, and TB grafts showed a fan shape approaching the tibial attachment, which most closely resembled the natural ACL of the three methods.

Another important finding for the second research question was that the high signal-intensity area was present in PLB images between the bone tunnel and the graft around the femoral tunnel aperture, especially in DB and TB reconstruction. Some authors have described relatively poor graft-to-tunnel healing in the PLB compared to AMB for these procedures [2, 25, 35]. The authors assessed the grafts arthroscopically and the backside of the grafts seemed to remain unevaluated. The results of our study showed the high signal-intensity lesion was located superoposterior to the graft, and taken together, these results indicate graft-to-bone healing was relatively unsatisfied in the PLB. These poor results in the PLB images might be due to two factors, including length change of the graft and graft fixation methods. The PL bundle shows greater length change during extension–flexion movement than the AM bundle [15], and the PL bundle could be susceptible to the bungee-cord effect or the windshield-wiper motion. In addition, use of the Endobutton might affect these unfavorable phenomena. A histological study by Nebelung [23] showed that granulation tissue was present between the graft and the bone tunnel in hamstring ACL reconstruction with Endobuttons. Additionally, a clinical study by Mae et al. [18] revealed a significant difference in the incidence of postoperative migration of the buttons between AM and PL grafts in DB reconstructions with Endobuttons. Although the poor results in PLB images of DB and TB reconstruction have not yet led to clinical failures, further follow-up analysis is required to elucidate clinical relevance.

In contrast, PLB images of SB grafts rarely showed these high signal-intensity lesions, suggesting more favorable graft-to-tunnel healing at the femoral side. This might be due to a lower excursion pattern in the posterolateral portion of the SB graft because the femoral tunnel of the